Available online at www.sciencedirect.com

ScienceDirect

journal homepage: www.elsevier.com/locate/he

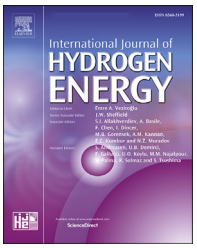

Electronic conductivity of catalyst layers of polymer electrolyte membrane fuel cells: Through-plane vs. in-plane

Mohammad Ahadi [a], *Mickey Tam* [b], *Jürgen Stumper* [b], *Majid Bahrami* [a,*]

[a] *Laboratory for Alternative Energy Conversion (LAEC), School of Mechatronic Systems Engineering, Simon Fraser University, Surrey, BC V3T 0A3, Canada*

[b] *Automotive Fuel Cell Cooperation Corp., 9000 Glenlyon Parkway, Burnaby, BC, V5J 5J8, Canada*

ARTICLE INFO

Article history:
Received 17 September 2018
Received in revised form
6 November 2018
Accepted 3 December 2018
Available online 11 January 2019

Keywords:
Polymer electrolyte membrane fuel cell
Catalyst layer
Electronic conductivity
Microstructure
Anisotropy
Structure-property correlations

ABSTRACT

In this work, novel procedures are developed to measure in-plane and through-plane electronic conductivities of catalyst layers (CLs) for polymer electrolyte membrane fuel cells. The developed procedures are used in a parametric study on different CL designs to investigate effects of different composition and fabrication parameters, including ionomer to carbon weight ratio (I/C ratio), dry milling time of the catalyst powder, and drying temperature of the catalyst ink. Results show that CLs have anisotropic electronic conductivity with through-plane values being three orders of magnitude lower than the in-plane values. The reason for this anisotropy is speculated to be alignment of fibrillar nanostructures of ionomer by large shear forces during coating, which could result in better carbon-carbon contact in the in-plane direction. A simple order of magnitude analysis shows the significance of poor through-plane conduction for fuel cell performance.

Introduction

Polymer electrolyte membrane fuel cells (in short PEM fuel cells or PEMFCs) are considered one of the alternative technologies for sustainable clean power generation due to their promising features, such as potentially zero greenhouse gas emissions, high efficiency, and abundance of their fuel source, i.e. hydrogen, which could be produced from various sources including electrolysis of water, reformation of hydrocarbons, and decomposition of hydrogen carrier chemical compounds [1–6]. PEMFCs generate power by combining hydrogen and oxygen through two half reactions occurring inside two respective catalyst layers (CLs), which are microporous materials and parts of a membrane electrode assembly (MEA). The final electrochemical reaction between hydrogen and oxygen in a PEMFC is exothermic, directly affecting the performance and degradation of the PEMFC by affecting local temperature variations inside the MEA. A considerable amount of Joule heating also occurs in the MEA components (~31% [7]), including the CLs where all the electron generation/

* *Corresponding author.*
E-mail addresses: mahadi@sfu.ca (M. Ahadi), mickeytam@gmail.com (M. Tam), jurstuju@gmail.com (J. Stumper), mbahrami@sfu.ca (M. Bahrami).

https://doi.org/10.1016/j.ijhydene.2018.12.016
0360-3199/

Nomenclature

Symbols and variables

A	Surface area (m^2)
$\mathscr{E}$	CL thickness utilization factor
ECR	Electronic contact resistance (Ω)
h	Thickness (m)
I	Current (A)
I/C	Ionomer to carbon weight ratio
L	Length (m)
m	Mass (kg)
n	Number of samples
R	Resistance (Ω)
R'	A constant residual resistance (Ω)
R^2	Coefficient of determination
t	Time (hr)
U	Velocity ($m.s^{-1}$)
V	Electric potential (V)
W	Width (m)

Greek Letters

Δ	Difference operator
μ	Viscosity (Pa·s)
ρ	Volumetric mass density ($kg \cdot m^{-3}$)
σ	Electronic conductivity ($S \cdot m^{-1}$)

Subscripts

b	Bulk
C	Carbon
cell	Cell
cl	Catalyst layer
ink	Catalyst ink
ip	In-plane
p	Probe
Pt	Platinum
rod	Coating rod
tot	Total
tp	Through-plane

consumption occurs. Accordingly, in-depth knowledge of electronic conductivity of CLs is needed for performance and degradation analysis/optimization of PEMFCs. Further, electronic conductivity test may be used as a forensic tool for assessing degradation level (e.g. carbon corrosion [8–11]) and structural defects (e.g. cracks); cracks in CLs could be created due to operational degradation [12–14] or due to certain conditions during CL manufacturing processes, e.g. low ionomer content of the ink, low drying temperature, and large thickness of the coating. However, only a few studies in literature have focused on electronic conductivity of CLs, in part due to measurement challenges associated with small CL thicknesses (~2–8 μm). Specifically, the literature lacks systematic measurement procedures for: i) effective deconvolution of the CL bulk resistance from its substrate/interfaces, and ii) separate measurement methods for through-plane and in-plane values. The electronic conductivity measurement methods available in the literature are effective methods (see Refs. [14–16]) using measurement techniques which assume isotropy for CLs (e.g. van der Pauw method [17,18]); this assumption may not be valid for cracked CLs or in case of microstructural inhomogeneities. Moreover, reported values in the literature are up to two orders of magnitude different [14–16,19] (also see Fig. 1), which could be originated from the effective nature of the used measurement methods, yielding a combination of in-plane and through-plane values.

In this work, novel procedures are proposed for measuring through-plane and in-plane electronic conductivity of CLs, and a parametric study is performed on the conductivities to examine effects of different compositions and fabrication parameters. The present study shows that CLs have notably different conductivities in different directions, indicating an anisotropic microstructure.

Experimental study

Substrate selection

The substrate resistance is in parallel to the CL resistance in the in-plane tests and in series in the through-plane tests. Thus, to minimize the substrate effect in the tests, an insulating substrate was needed for the in-plane tests, while a highly conductive substrate was needed for the through-plane tests. Two available substrates were: i) ethylene tetrafluoroethylene (ETFE) sheet which was insulating and used as a decal in constructing catalyst-coated membranes (CCMs) in a process called "decal transfer" [20–24], and ii) aluminum (Al) foil which was highly conductive and normally used as a substrate/backing for ex-situ measurements [20,25]. A systematic investigation of microstructural parameters, including porosity, pore size distribution, surface roughness, crack density, crack aspect ratio, and surface and bulk chemistry showed that CLs of the same ink coated on ETFE and Al substrates had the same microstructure. Ref. [20] also confirmed that CLs of the same ink coated on these substrates had the same through-plane thermal conductivity. Accordingly, in this work, CL samples were coated on ETFE for in-plane tests and on Al for through-plane tests.

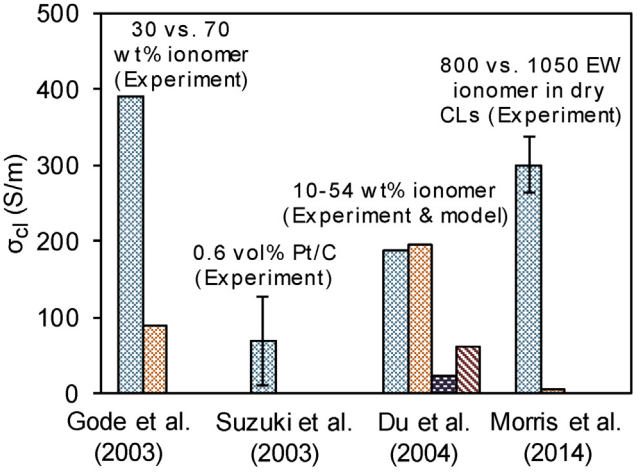

Fig. 1 – Literature data on electronic conductivity of CLs (from Refs. [14–16,19]), showing up to two orders of magnitude difference between the data from different sources.

Table 1 – Fabrication details of different CL designs coated for the study.

Design #	I/C ratio	Dry milling time (hr)	Drying temperature (°C)
1	1.1	0 (None)	55
2	0.7	48	55
3	0.9	48	55
4	0.7	24	55
5	1.1	48	55
6	0.9	24	55
7	1.1	48	24 (Room temperature)
8	1.1	0 (None)	24 (Room temperature)

Ink preparation and coating

CLs with different compositions and microstructures were produced and measured. Composition was altered by changing the weight (wt) ratio of ionomer to carbon (I/C). A catalyst powder made from platinum (Pt) nanoparticles supported on partially graphitized carbon (C) nanoparticles (Pt/C catalyst) with 50 wt% of Pt was used in all the inks. In addition to changing the I/C ratio, different microstructures were made by: i) dry ball-milling (or in short dry-milling) the Pt/C catalyst powder to compact the Pt/C catalyst aggregates (before making the ink) as a way to reduce the porosity without changing the composition, and ii) changing the drying temperature of the ink (after coating) whose obvious effect was inducing cracks. In the dry milling step, dry catalyst powder was grinded by zirconia balls on a jar mill for a desired length of time. Ball milling has been extensively used for changing the structure of graphitic materials [26–34]. During ball milling of the aggregates, all carbon blacks achieve a maximum level of breakdown in less than 30 min leading to surface area enlargement; further ball milling leads to collapse of the porous structure, new bonding between the particles, and compacting the aggregates into microagglomerates with less surface area [34,35]. To be consistent with the CL literature, in this work, the word "aggregate" is used to refer to a group of Pt/C particles covered by ionomer film, and the word "agglomerate" is used to refer to a Pt/C aggregate and its surrounding ionomer film together. Thus, a CL could be described as a configuration of agglomerates and pores. In the carbon black literature, however, different definitions are used for aggregates and agglomerates (e.g. see Ref. [36]).

Catalyst ink was prepared by mixing the (dry-milled) Pt/C catalyst powder with water, solvent, and ionomer. The prepared ink was coated onto one side of ETFE sheets for in-plane tests and Al foils for through-plane tests, using a Mayer bar coater. To enable deconvolution of the CL bulk signal in through-plane tests, different thicknesses of the same ink were made on Al. Table 1 shows fabrication details of different CL designs coated for this study. Fig. 2 shows a schematic of the CL fabrication process together with scanning electron microscope (SEM) images of three designs, indicating the very different structures of the coatings. One point is worth mentioning regarding the SEM images of Fig. 2. The SEM images were acquired using the backscattered electron (BSE) detector. Since heavy elements (i.e. elements with high atomic numbers) backscatter electrons more strongly than light elements (i.e. elements with low atomic numbers), heavy elements appear brighter in SEM images acquired using the

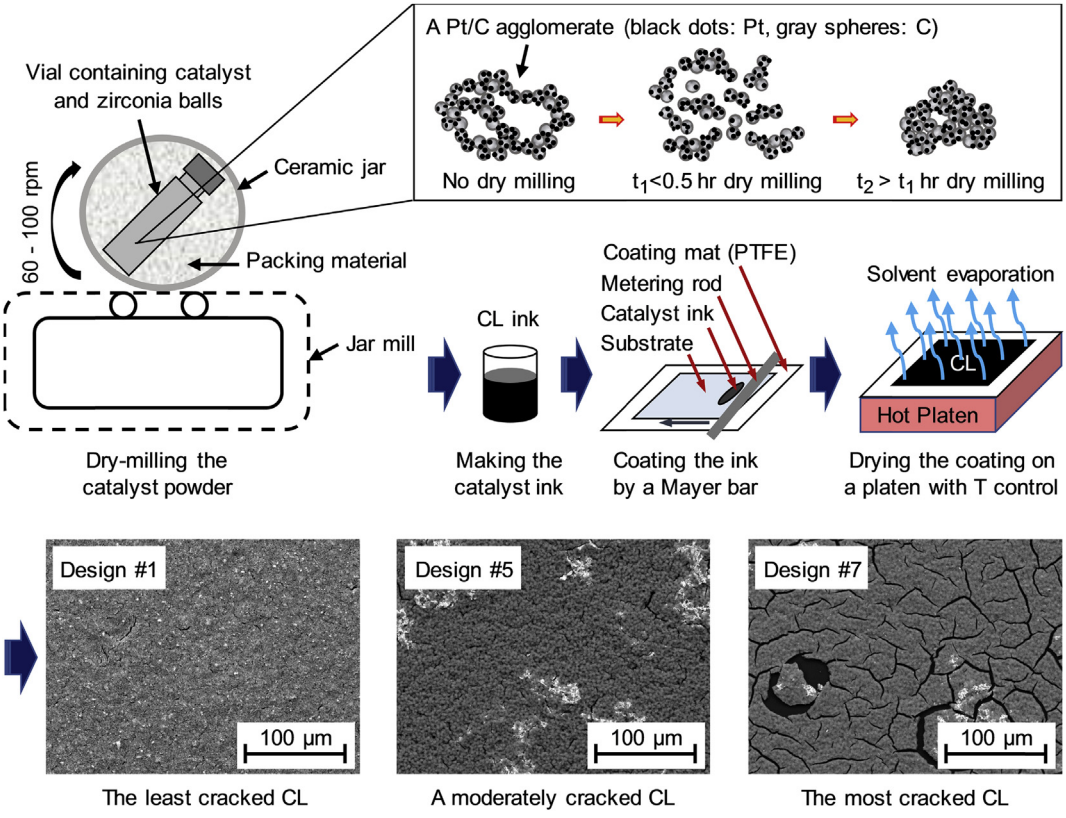

Fig. 2 – Schematic of the CL fabrication process and SEM images of three designs showing different microstructures.

BSE detector. Thus, the white marks observed in the images of designs #5 and #7 in Fig. 2 are, in fact, made of the heavy element of Pt. This shows that, for these CL designs, some Pt particles could be removed from their carbon support by long dry milling and could make localized Pt aggregates (i.e. the white marks in the images). This effect was only observed for designs #2, #3, #5, and #7, whose catalyst powder was dry-milled for 48 hours. The designs with 0 or even 24 hours dry milling time, on the other hand, did not show this effect. As also mentioned in Ref. [37,38] such Pt detachment leads to loss of electrochemical surface area and, thus, lower catalytic activity, which is detrimental to fuel cell performance. Thus, aggressive dry milling of the catalyst powder is not desirable in general.

Thickness and porosity measurements

Thicknesses of the CL samples were needed for deconvoluting the conductivities from the resistance data, and porosities were needed to track changes in the microstructure as the fabrication parameters were changed. Thickness and porosity were measured using two methods for cross-checking: i) SEM, using a Philips XL30 Environmental SEM for measuring the thickness (see Ref. [20] for more details regarding the SEM thickness measurements), which was turned into porosity using the known densities of the components and areal Pt loading measured by an X-ray fluorescence (XRF) analyzer (Themo Scientific, Niton XL3t) (see Ref. [16] for details of porosity calculations), and ii) a buoyancy method similar to the technique used for measuring gas diffusion layers (GDLs) introduced in Ref. [39]. The two methods agreed well with each other.

Crack characterization

As SEM imaging of CL cross sections showed, most of the cracks would go deep through the whole CL thickness, dividing the coating into interconnected and separate catalyst islands. Thus, resistance of cracks acts in parallel to the CL bulk resistance in the through-plane direction and in series in the in-plane direction. Accordingly, cracks were expected to more significantly affect the in-plane conductivity with less effects on the through-plane conductivity. One exception would be losing too much conductive surface area in a highly cracked sample, in which case, the effects on the through-plane conduction would also be significant. To understand the effects, cracks were characterized by: i) areal density defined as areal percentage of the cracks on the CL surface, and ii) aspect ratio defined as the long over the short edge ratio. Crack density quantifies volume fraction of cracks (considering their penetration through the whole thickness), whereas crack aspect ratio quantifies shape of cracks. Both of these properties appear in modeling the in-plane electronic and thermal conductivities of CLs, as exercised by the authors in a separate work. Thus, effective characterization of cracks is hinged on measuring and analyzing both of these properties. These parameters were measured by processing surface SEM images of CLs using Fiji ImageJ software (available in the public domain).

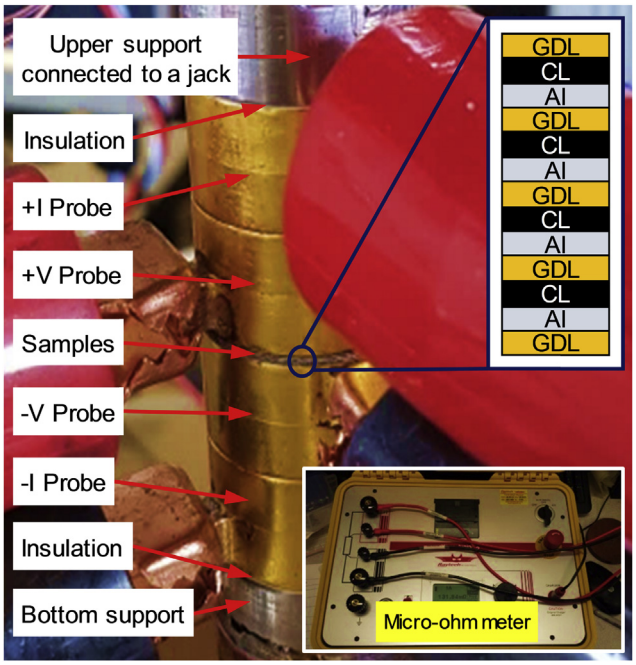

Fig. 3 – Custom-made through-plane electronic conductivity testbed and sample configuration (the upper inset on the right).

Electronic conductivity tests

Four-point probe measurements of resistance were performed using a Micro Junior 2 micro-ohm meter (Raytech, USA) using a DC current. Calibration of the device was confirmed with ±3% error using 0.01–10^5 Ω standard resistors. Applicability of Ohm's law for CLs was confirmed by the very linear current-voltage characteristic in both through-plane and in-plane directions.

Through-plane tests

Four custom-made gold-plated probes were used as sample holders for through-plane tests. Samples were cut into one-inch circles by a punch to fit the circular shape of the probes. The samples were then clamped between the probes attached to corresponding current and voltage leads of the micro-ohm meter. The whole samples-probes sandwich was put under pressure by a pneumatic jack to control the contact pressure (see Fig. 3). Calibration of the through-plane testbed was ensured by measuring GDL samples and obtaining values which were in good agreement with the manufacturer's data. Further, only a few μΩ was measured by the through-plane setup when no sample was mounted; this showed minimal contribution from the probes and interfaces between them, when compared to through-plane resistance of the samples which was in the order of 1Ω.

Our through-plane resistance measurements of CL samples showed that electronic contact resistances (ECRs) at the interfaces played a significant role in the total resistance and would compromise repeatability of the tests; this issue was also mentioned by Ref. [14]. The ECRs were originated from imperfect contact between the surfaces. Accordingly, effort was made

to find a material with high electronic conductivity which could reduce the ECRs at the interfaces by deforming plastically and filling the gaps. Among all the tested materials, GDLs proved to be the best. Their through-plane resistance was two orders of magnitude lower than the CL samples, and they significantly reduced the ECRs and made the measurements repeatable. In the optimum sample configuration, GDLs were used at every interface in the setup, except at the interfaces between the probes whose contribution was significantly minimal (only a few μΩ). Multiple CL samples (with GDLs at every interface) were stacked and measured to reduce uncertainty in the data by increasing the amount of catalyst in the setup (see the sample configuration shown schematically in Fig. 3).

Total through-plane resistance measured for a stack consisting of n samples with GDLs at every interface could be expressed as:

$$R_{tot,tp} = nR_{cl,b,tp} + R' = \frac{nh_{cl}}{\sigma_{cl,tp}A_p} + R' = \frac{h_{cl,tot}}{\sigma_{cl,tp}A_p} + R' \quad (1)$$

where $R_{cl,b,tp}$ shows through-plane bulk resistance of a CL, and R' is summation of all the measured resistances except for the bulk of the CLs (i.e. Al substrates, GDLs, probes, and ECRs in between); h_{cl} and $\sigma_{cl,tp}$ are thickness and through-plane conductivity of the CL, respectively; $h_{cl,tot} = nh_{cl}$ is total thickness of the CLs in the stack, and A_p is area of the probes covering the stack (the same as area of a sample). As indicated by Eq. (1), $R_{tot,tp}$ is a linear function of $h_{cl,tot}$. Accordingly, by measuring multiple h_{cl}'s (or multiple $h_{cl,tot}$'s), $\sigma_{cl,tp}$ and R' could be deconvoluted from a linear regression analysis of the $R_{tot,tp}$ vs. $h_{cl,tot}$ plot ($\sigma_{cl,tp}$ from the slope and R' from the intercept). Thus, effects of all the substrates and interfaces are deconvoluted from the final conductivity results because those effects are bundled in R'. Typical resistance measurements for different CL thicknesses yielded fairly straight lines for $R_{tot,tp}$ vs. $h_{cl,tot}$ plots with $R^2 \sim 0.98$ and even better.

In-plane tests

In-plane tests were performed using a custom-made in-plane sample holder, shown in Fig. 4, integrated with the micro-ohm meter. The sample holder consisted of two metallic jaws, for clamping strips of samples, and four sliding plastic frames, enabling adjustment of the sample length between the probes. GDLs were used between the clamps and the sample to protect the CL surfaces from the metallic jaws and reduce ECRs in the tests. In-plane resistance of the GDLs was orders of magnitude lower than the CLs and, therefore, would fall into the error range and could be neglected. Accordingly, total in-plane resistance measured for a sample could be expressed as:

$$R_{tot,ip} = R_{cl,b,ip} + ECR = \frac{L_{cl}}{\sigma_{cl,ip} \cdot h_{cl} \cdot W_{cl}} + ECR \quad (2)$$

where $R_{cl,b,ip}$ shows in-plane bulk resistance of the CL; $\sigma_{cl,ip}$ is in-plane conductivity of the CL; L_{cl} is probed length (length of the sample between the clamps), and W_{cl} is width of the CL strip. Similar to Eq. (1), measuring at least two lengths of a sample would enable deconvolution of $\sigma_{cl,ip}$ and ECR by a linear regression analysis of the $R_{tot,ip} - L_{cl}$ plot. Typical measurements for different CL lengths yielded fairly straight lines for $R_{tot,ip}$ vs. L_{cl} plots with $R^2 \sim 0.99$.

Results and discussion

Microstructural parameters: porosity, crack density, and crack aspect ratio

Fig. 5 shows microstructural parameters for different CL designs, including porosity, crack density, and crack aspect ratio. Fig. 5a–c show that porosity decreases with increasing the I/C ratio and dry milling time but does not change with drying temperature. Reasons behind the decreasing trends could be: i) filling more pores with ionomer by increasing the I/C ratio, and ii) more compactness of the Pt/C aggregates with increasing the dry milling time. Fig. 5d–f show that surface crack density decreases with increasing the I/C ratio and drying temperature but increases with increasing the dry milling time. Reasons behind these trends could be: i) enhancing structural integrity of the CL by increasing the I/C

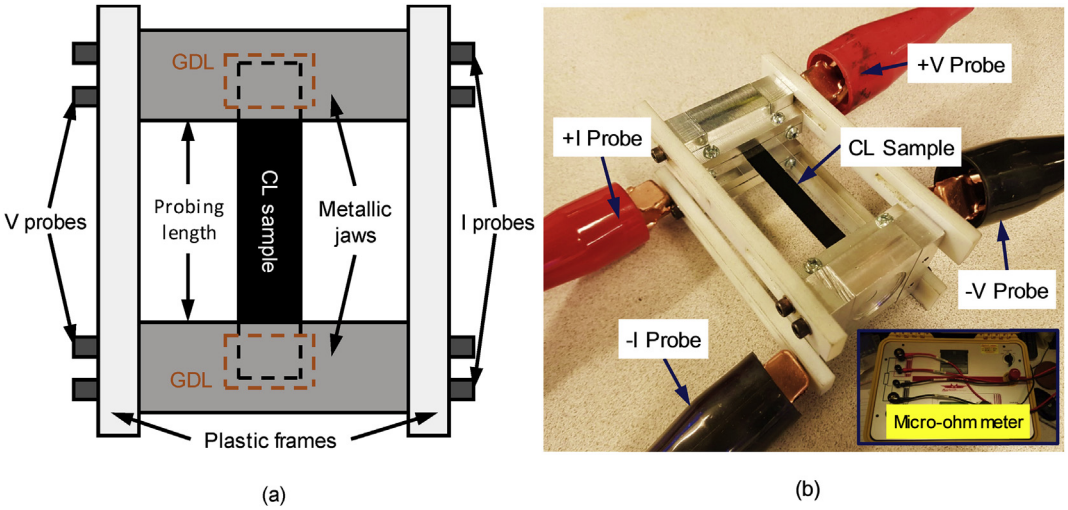

Fig. 4 – In-plane electronic conductivity testbed and sample holder: (a) a schematic of the in-plane sample holder, (b) the in-plane sample holder integrated with the micro-ohm meter.

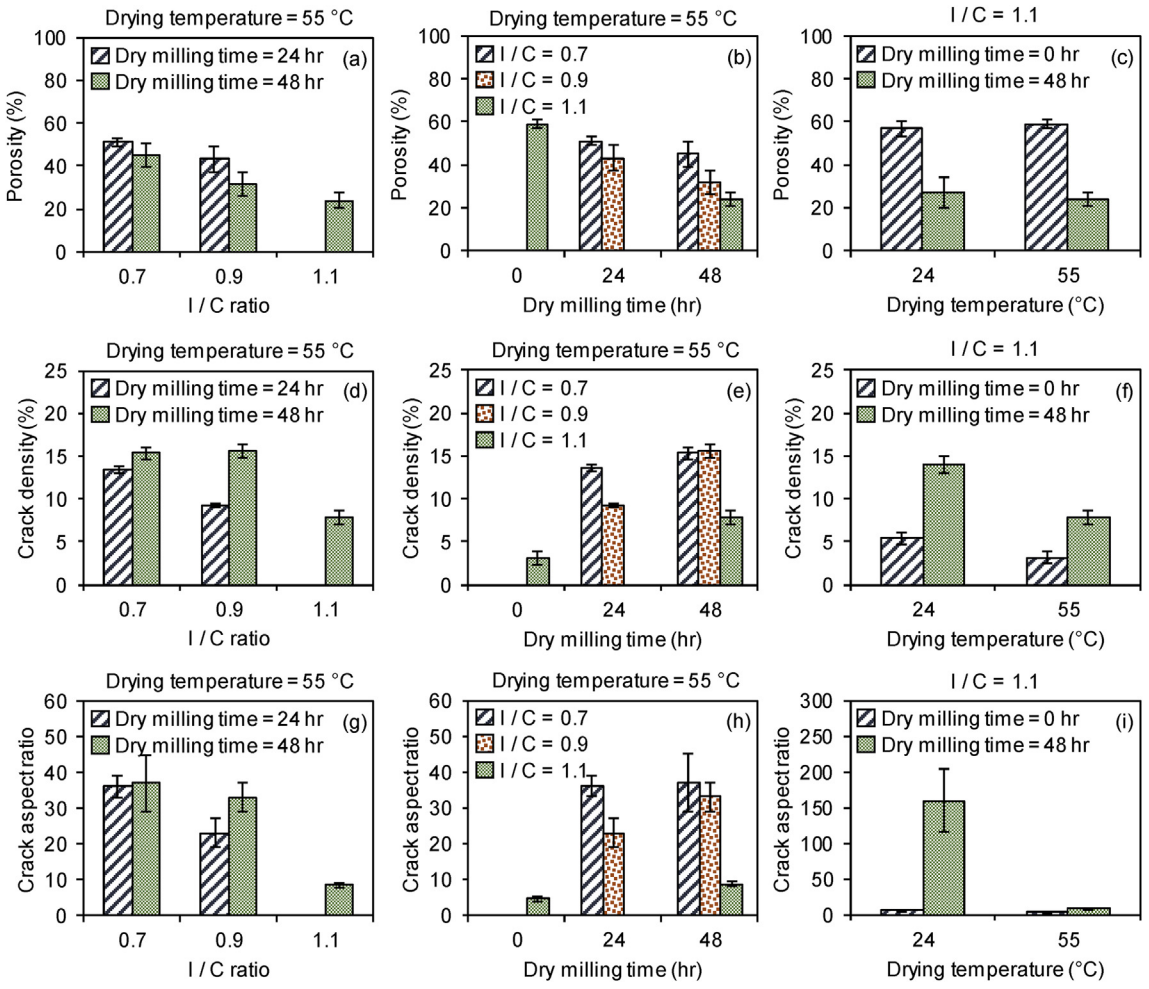

Fig. 5 – Microstructural parameters for different CLs: (a–c) porosity, (d–f) crack density, (g–i) crack aspect ratio.

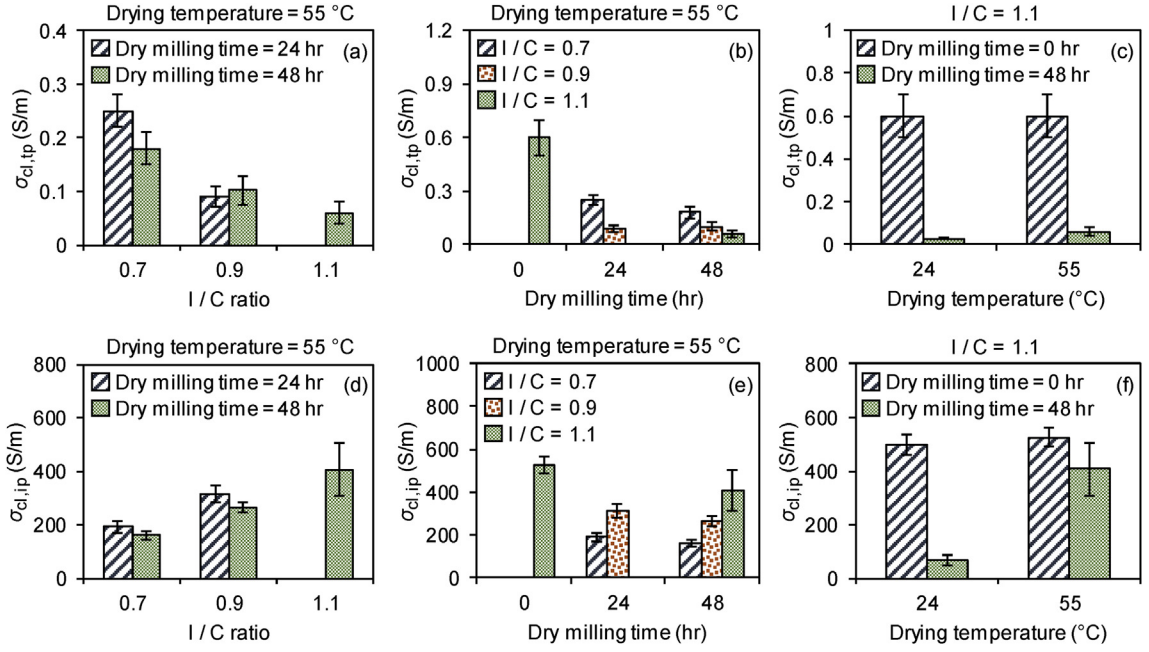

Fig. 6 – Electronic conductivity of different CL designs: (a–c) through-plane vs. (d–f) in-plane.

ratio (i.e. more ionomer as a binder), ii) quicker solidification of ionomer when the ink dries by increasing the drying temperature, giving less time to the aggregates to move around and rearrange themselves, and iii) smaller contacts between the aggregates (hence weaker to forces from the solidifying ionomer) by increasing the dry milling time due to increasing sphericity of the particles [31].

Fig. 5g–i show that crack aspect ratio follows the same trends as the crack density does; the same reasons mentioned for the trends of crack density apply here for explaining the trends of crack aspect ratio. Most of the CLs had aspect ratios below 40 except for design#7 with I/C = 1.1, 48 hr dry milling time, and 24 °C drying temperature, which had a crack aspect ratio of ~160. This very high aspect ratio was a direct result of long dry milling and low drying temperature of the ink. As shown in Fig. 5, this CL had one of the highest crack densities and one of the lowest porosities as well.

Through-plane vs. in-plane electronic conductivity

Fig. 6 shows through-plane vs. in-plane electronic conductivity for all the designs. As shown in Fig. 6, through-plane values are generally three orders of magnitude lower than the in-plane values, which indicates anisotropy of the CLs. This anisotropy in microstructure is discussed in the next section.

Fig. 6a and b show that through-plane electronic conductivity decreases with increasing the I/C ratio and dry milling time. Reasons behind these decreasing trends could be speculated as:

i) The added ionomer may affect the contact points between the carbon particles of neighboring agglomerates in the through-plane direction by penetrating between them and, thus, making the contact areas smaller. More justifications are provided in the next section when the anisotropy is explained.
ii) Carbon particles may go through a transition from a polyhedron shape to a spherical shape by dry milling [31]. Such a transition may result in reduction in the size of contact areas between the particles from flat facets of the polyhedrons to point contacts between the spheres, hence leading to reduction in the conductivity. Similar bending and rounding effects have been observed for ball milling of other graphitic materials [26,28].

Fig. 6c shows that increasing the drying temperature increases the through-plane conductivity for dry milling time of 48 hr but does not change the conductivity for 0 hr dry milling time. The observed increase for the 48 hr dry milling time could be explained based on the very different structure of the CL with I/C = 1.1, 48 hr dry milling time, and 24 °C drying temperature (i.e. design #7). As shown in the SEM surface image of design #7 in Fig. 2, this design lost a considerable amount of CL area to surface cracks; further, the free spaces left from detachment of big chunks of catalyst in design #7 could significantly increase through-plane constriction resistances through this design. However, such dramatic structural changes were not observed for the CLs with 0 hr dry milling time (and I/C = 1.1).

In Fig. 6d, a different trend with I/C ratio is observed for the in-plane conductivity; unlike the through-plane conductivity, it increases with increasing the I/C ratio due to reduction in the surface crack density and crack aspect ratio (see Fig. 5). Addition of more ionomer results in better structural integrity of the CL in the in-plane direction (hence fewer and smaller cracks and more carbon-carbon contacts). As discussed in the next section, experiments show that ionomer must not penetrate much between the in-plane connections of the aggregates; thus, unlike the through-plane electronic connections, there should be no negative effect from ionomer on the in-plane electronic connections. Fig. 6e and f show the same trends for in-plane conductivity as observed for effects of dry milling time and drying temperature on the through-plane conductivity. In addition to the reasons mentioned for these trends for the through-plane conductivity, the following factors could negatively affect the in-plane conductivity: i) increasing the crack density and crack aspect ratio by increasing the dry milling time (in addition to increasing sphericity of the particles), and ii) significant increase in the crack aspect ratio (in addition to crack density) by decreasing the drying temperature for 48 hr dry milling time.

Results of Fig. 6 show that designs #1 and #8 with I/C = 1.1 and 0 hr dry milling time were the most conductive CLs among all the designs, which is counterintuitive considering that these CLs had the highest I/C ratio (i.e. the highest ionomer content) and highest porosities among all the designs. The highest conductivities of these CLs were results of their specific microstructure dictated by their specific composition and fabrication, as discussed above. This shows that a simple intuitive relationship between the conductivity and porosity or ionomer content of CLs does not exist and clarifies the need for developing an in-depth understanding of structure-property correlations, which is one of the main goals of this work.

Explaining the observed anisotropy in electronic conductivity

To explain the anisotropy, a discussion is needed first regarding the limiting factor of electron conduction in CLs. The only components of a CL which could conduct electrons are C and Pt particles. The Pt particles, however, have a small volume fraction compared to the C particles; the ratio between the volume of Pt and C can be obtained as $(m_{Pt}/m_C) \times (\rho_C/\rho_{Pt})$ which is calculated to be ~7%, considering the 1:1 mass ratio of Pt to C in the used Pt/C catalyst and densities of ~1,600 $kg \cdot m^{-3}$ for porous C particles and ~21,450 $kg \cdot m^{-3}$ for Pt particles. Further, the current trend in literature for optimizing CLs is to reduce their cost by decreasing their Pt loading, meaning that the volume fraction of Pt particles could fall below 7%. Thus, Pt particles do not contribute much in conduction of electrons as they do not occupy much volume in CLs. Micrographs of Pt/C aggregates available in literature also confirm this claim by showing Pt particles as tiny particles sparsely covering the surface of C aggregates (for example see Ref. [38]). Therefore, electron conduction in CLs should be determined by the properties of the carbon phase. Inside the aggregates, C particles are strongly fused together by covalent bonds [35,40–42], which

means that bulk conductivity of the aggregates should be fairly high. Accordingly, conduction of electrons in CLs should be limited by carbon-carbon contacts between aggregates of neighboring agglomerates.

Thus, the only way to explain the anisotropy in CLs is if the Pt/C aggregates were connected together considerably better in the in-plane direction than the through-plane direction. To test this hypothesis on a CL, effort was made to weaken the connections between the aggregates by hydrating the CL ex-situ and examining its effects on the through-plane and in-plane electronic conductivities; hydration was expected to weaken the connections as a consequence of ionomer swelling. For this purpose, samples of design #1 (i.e. the CL with the highest electronic conductivity in both directions) were kept under 80 °C deionized water for 1 hr to allow penetration of water into the pores and ionomer; the 80 °C temperature was used to reduce the surface tension of water and allow its penetration into the pores. The same strategy was used by Ref. [43] for hydrating GDLs. Experiments showed that CLs almost completely lost their through-plane conductivity at ~16–20% water uptake in an irreversible way when hydrated in the way explained, whereas the loss in in-plane conductivity was only ~50%. This showed that as hydration occurred, ionomer swelled and took adjacent Pt/C aggregates apart from each other, thereby weakening the contacts between them. Observing a nearly complete loss in the through-plane conductivity revealed that adjacent Pt/C aggregates must have had very weak through-plane connections, which completely broke as the CLs were hydrated, but much stronger in-plane connections, of which only ~50% broke by hydration. However, in real operation of a fuel cell, all the cells are under ~1.5–3.0 MPa compression when hydration occurs in-situ as a result of the electrochemical reaction, and we can speculate that these high contact pressures would hold the structural integrity of the CLs and would prevent the collapse of CL through-plane electronic conductivity observed during our ex-situ hydration tests. Thus, the results of the ex-situ hydration tests conducted in this work should strictly be regarded as proofs for different contacts of Pt/C aggregates in the in-plane and through-plane directions, and the conductivity results for the hydrated CLs are not relevant for fuel cell performance. It is worthy to clarify here that the observed collapse of the through-plane electronic conductivity must have been originated from a corresponding collapse in the microstructure, which we can predict due to observing its effects on the through-plane electronic conductivity. However, as observed by naked eyes, the CLs remained intact during and after the ex-situ hydration tests, and they were neither scratched nor damaged; they also remained stuck on their substrates and did not flake off. Ref. [16] conducted electronic conductivity measurements on CLs at elevated relative humidity (RH); they also observed reduction in electronic conductivity by increasing the gas RH and attributed the losses to ionomer swelling.

Speculations could be made for reasons behind the very different contacts of Pt/C aggregates in the through-plane and in-plane directions, based on the used coating method in this work and behavior of ionomer in the catalyst ink under shear. Mayer-bar coating was used in this work for producing CLs due to its high resemblance to the roll-coating process used in industry for mass production of CLs. In this process, a coating rod would move with a speed of ~0.1 $m \cdot s^{-1}$ over the ink to spread it on the substrate. In this work, viscosity of the ink was not measured. However, taking the viscosity value of 2.75 Pa·s from Ref. [44], approximating the applied shear by the coating rod on the ink as $\mu_{ink} U_{rod}/h_{ink}$ (μ_{ink}: ink viscosity; U_{rod}: coating speed; h_{ink}: ink thickness) and assuming a thickness of ~20 μm for the ink (higher than the dried CL thicknesses), a shear force of ~14,000 $N \cdot m^{-2}$ is calculated which is a considerable value. On the other hand, ionomer, as a polymer electrolyte, has a fibrillar structure which could be aligned in presence of shear forces along the shear direction [45–51]. Further, hydration of ionomer nanofibers in the ink could produce a one-dimensional paracrystalline lattice, separated by polymer layers, as shown by Ref. [52] for hydrated Nafion; this could further help alignment of ionomer nanofibers along the shear direction by straightening the hydrated nanofibers like hoses filled with water. Several researchers have reported effects of this alignment in ionomers on physical properties. For instance, Ref. [51] showed highly anisotropic proton conduction in block copolymer electrolyte membranes aligned by applying electric field and shear, and Ref. [53] showed highly anisotropic ionic conductivity of block copolymer membranes aligned in presence of magnetic field.

Accordingly, it is speculated that alignment of hydrated ionomer nanofibers in presence of high shear forces during Mayer-bar coating may be the main reason for having weak through-plane connections between the aggregates. It is speculated that alignment of ionomer nanofibers in the in-plane direction (i.e. the shear direction) may lead to penetration of ionomer into the through-plane contacts between the aggregates, thereby weakening the contacts and increasing their chance of breakage by ionomer swelling. This may further explain the observed complete loss of through-plane conductivity by hydrating the CLs; as hydration occurred, it is possible that the ionomer at the through-plane contact regions between the aggregates swelled and disconnected the through-plane electronic connections. The in-plane electronic connections, though, were not affected as much as the through-plane connections perhaps due to the much lower amount of ionomer at the in-plane contacts.

As noted by Refs. [46,50], ionomer fibrillar structures have a diameter of 3–4 nm and a length on the order of ~100 nm

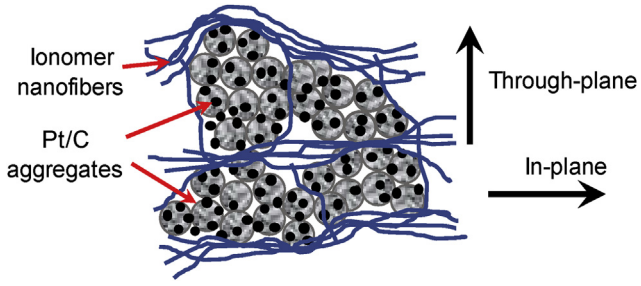

Fig. 7 – The proposed model for arrangement of ionomer nanofibers around the Pt/C aggregates in a CL (small black spheres: Pt; larger spheres: C), suggesting existence of more ionomer nanofibers along the in-plane direction due to alignment by shear during coating.

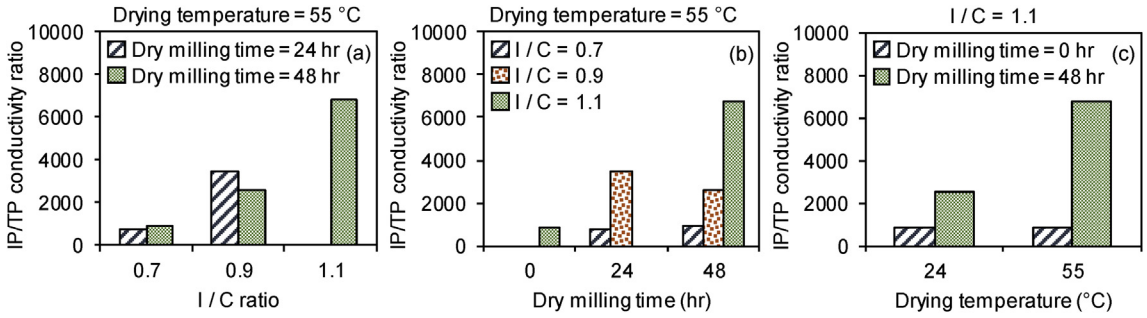

Fig. 8 – In-plane (IP) to through-plane (TP) conductivity ratio for different CL designs.

which is well comparable with the aggregate size of 100–300 nm (as we measured; this range was also reported in Refs. [54–56]). This suggests another speculation for effect of hydration on the in-plane electronic conductivity; it is possible that each fibrillar nanostructure of ionomer, after getting aligned in the in-plane direction (still a speculation), adheres to two neighboring aggregates in the in-plane direction and binds them together, thereby providing structural integrity for the CL in the in-plane direction, as shown schematically in Fig. 7. After the ink dries, these fibrillar nanostructures may contract in length and enhance the in-plane contacts between the aggregates. Thus, a probable mechanism for reduction of the in-plane conductivity by hydration could be loosening the long ionomer strands holding the aggregates in the in-plane direction.

One argument regarding the proposed model in Fig. 7 is that the proposed structural anisotropy of the ionomer phase should also be seen in protonic conductivity. However, separate measurements of protonic conductivity of CLs in different directions have not been reported in literature yet, and the existing protonic conductivity measurements have assumed negligibility of the electronic resistance of the CLs in their analyses [14,57–59]. The through-plane electronic conductivity measurements of this work show that such an assumption may not be valid. The measurements of this work could be served as a first step toward development of more accurate techniques for protonic conductivity measurements in different directions, which may further be used to examine the validity of the proposed model in Fig. 7 by investigating the anisotropy for protonic conductivity. Another aspect is that such anisotropy in protonic conductivity is speculated to be detrimental to fuel cell performance because, according to the model proposed in Fig. 7, most of the ionomer nanofibers would be aligned in the in-plane direction. It is probably more beneficial to have ionomer nanofibers aligned in the through-plane direction to transfer protons between the membrane and the catalyst sites inside the CLs. Investigation of these issues is beyond the scope of this study and is only suggested here as a future work.

Another argument is that since Mayer bar coating is a directional method, which performs the coating in only one direction, one may expect to see difference between in-plane electronic conductivity/resistance values along the machine (or coating) direction and measurements along the direction perpendicular to the coating direction. However, experiments with CL strips of design #1 showed no difference between the two directions, which is counterintuitive and demands a more in-depth analysis of the CL microstructure. This shows that the proposed model in Fig. 7 needs to be further confirmed/improved/modified through advanced ionomer visualization techniques, such as soft X-ray spectro-tomography introduced in Ref. [60]. This will help better understand the true 3D distribution of ionomer within the CL. The electronic conductivity measurements of this work provide a motivation for such more in-depth investigations.

Anisotropy trends

Anisotropy trends are revealed by plotting the ratio of in-plane (IP) to through-plane (TP) conductivity for different designs, as shown in Fig. 8. The graph shows that increasing the ionomer content leads to increase in the IP/TP anisotropy; this seems to make sense if we consider the ionomer as the lubricant and insulating material between the particles. More ionomer may lead to less particle-to-particle contact points in the TP direction after coating, perhaps due to shear/separation effect (see Fig. 7). Dry milling generally increases the anisotropy; for I/C = 1.1 (and 55 °C drying temperature), the increase is almost a factor of 8. Higher dry milling time may lead to smaller and rounder particles with less particle-to-particle contact points in the TP direction after coating, leading to an increase in anisotropy. The graph further shows that only for the dry-milled powder, the drying temperature has an effect. Higher drying temperature means faster drying, which "freezes" the after-coating structure. Thus, it appears that faster drying could better conserve/freeze the anisotropy for the dry-milled case. The reason for this observation is the much more significant augmentation in crack density and crack aspect ratio with slow drying for the dry-milled case (see Fig. 5f and i), which makes the IP conductivity significantly worse and closer to the TP conductivity (see Fig. 6c and f), thereby reducing the anisotropy in this case.

Significance of having a low through-plane electronic conductivity for CLs

Low magnitude of through-plane electronic conductivity of CLs could have significant impacts on the performance of PEM fuel cells. A simple order of magnitude analysis of the possible voltage drop across a CL clarifies the issue. In practice, only a

fraction of the CL thickness may be utilized in the electrochemical reactions due to mass transport limitations and other factors [61–66]. The utilized fraction of the CL thickness depends on operating conditions, CL composition, and balance between transport of species through the CL [62,64]. Accordingly, order of magnitude of the voltage drop across a CL could be obtained as $O(\Delta V_{cl}) \sim O(R_{cl,tp} I) \sim O(\{\mathscr{E} h_{cl}/(\sigma_{cl,tp} A_{cell})\} I)$, where ΔV_{cl} represents the voltage drop across the CL in [V], $R_{cl,tp}$ the CL through-plane resistance in [Ω], I the current in [A], $\mathscr{E}$ the utilized fraction of the CL thickness ($O(\mathscr{E}) \sim 0.1$ [62]), h_{cl} the CL thickness ($O(h_{cl}) \sim 10^{-4}$ cm), $\sigma_{cl,tp}$ the CL through-plane conductivity ($O(\sigma_{cl,tp}) \sim 10^{-3}$ S·cm^{-1}), and A_{cell} the cell area in $[cm^2]$. For a typical cell with $A_{cell} = 1\ cm^2$, output voltage of 700 mV, and current density of 1 A·cm^{-2}, this means having $O(\Delta V_{cl}) \sim O(10\ mV)$. In practice, this voltage drop could also be influenced by nonuniform distribution of the current density across the CL thickness [61–64]; for instance, similar calculations considering a linear distribution for current density across the thickness (as suggested by Ref. [64]) yields $O(\Delta V_{cl}) \sim O(5\ mV)$.

Accordingly, the exact value of voltage drop accross the CLs could be significant. This indicates a motivation to enhance the CL through-plane electronic conductivity; one way could be developing coating methods which won't prefer one direction to another. The exact value of share of CLs in the performance loss, however, should be obtained through a rigorous modeling of the performance, while considering precise values for other resistances, namely, protonic resistances of the electrolyte and CLs as well as resistances of the interconnects and contacts. Unfortunately, such a detailed breakdown of different resistances is not available at the moment. Further, there are two other complications regarding such a rigorous analysis:

i) As mentioned before, measurements of protonic conductivity of CLs in literature have been under the assumption of negligible electronic resistance for the CLs [14,57–59], which was questioned in this work.

ii) In this work, electronic conductivity was measured for fresh CLs, whereas in practice, CLs are conditioned before a fuel cell is made operational [57,58,67]. This could further change the morphology of the CLs and could affect their conductivity in operation.

Accordingly, more research is still needed in the above-mentioned areas to fill the existing knowledge gaps and enable a precise analysis of the different modes of ohmic loss.

Conclusions

In this study, novel procedures were developed to measure through-plane and in-plane electronic conductivities of PEM fuel cell CLs. The proposed procedures are not limited to CLs and could be used for similar conductive coatings. The developed procedures were then used to perform a parametric study on the conductivities for CL designs with different compositions and fabrication parameters. Results showed highly anisotropic electronic conductivity for all the CLs. The conductivities in different directions were highly dependent on the composition and fabrication parameters of the ink. Both conductivities showed the same trends with different parameters, except for ionomer content which negatively affected the through-plane conductivity but positively affected the in-plane conductivity. The observed anisotropy was speculated to be a result of alignment of ionomer nanofibers along the in-plane direction by high shear forces during coating. An order of magnitude analysis of voltage drop across a CL showed the significance of such losses and the need to enhance the through-plane conductivity by developing more efficient coating methods.

Other conventional coating methods to be considered include printing and spray-coating. However, it should be noted that such methods entail forcing the catalyst ink through small nozzles (with micrometer-size diameters) via applying pressure. Thus, the ink would again experience considerable shear forces from the walls of the nozzles, which could again lead to anisotropy. Nonetheless, trying such methods and investigating the effects on the in-plane and through-plane electronic conductivities is an interesting topic for future research and could reveal more details about the microstructure.

Acknowledgement

The authors would like to gratefully acknowledge financial support received from the Natural Sciences and Engineering Research Council of Canada (NSERC) through NSERC Collaborative Research Development Grant no. 31-614105. The authors also thank Dorina Manolescu from Automotive Fuel Cell Cooperation Corp. (AFCC) for assisting in making the inks and coating the CLs, Dr Jasna Jankovic from AFCC for her expert consultations regarding the aggregate microstructure, and Saeed Shokoya from SFU for his assistance in some of the electronic resistance tests during his undergraduate co-op program at SFU.

REFERENCES

[1] Ahmadi P, Kjeang E. Comparative life cycle assessment of hydrogen fuel cell passenger vehicles in different Canadian provinces. Int J Hydrogen Energy 2015;40(38):12905–17.
[2] Miyaoka H, Miyaoka H, Ichikawa T, Ichikawa T, Kojima Y. Highly purified hydrogen production from ammonia for PEM fuel cell. Int J Hydrogen Energy 2018;43(31):14486–92.
[3] Cifuentes B, Bustamante F, Conesa JA, Córdoba LF, Cobo M. Fuel-cell grade hydrogen production by coupling steam reforming of ethanol and carbon monoxide removal. Int J Hydrogen Energy 2018;43(36):17216–29.
[4] Sinigaglia T, Lewiski F, Martins MES, Siluk JCM. Production, storage, fuel stations of hydrogen and its utilization in automotive applications-a review. Int J Hydrogen Energy 2017;42(39):24597–611.
[5] Yapicioglu A, Dincer I. Performance assesment of hydrogen and ammonia combustion with various fuels for power generators. Int J Hydrogen Energy 2018;43(45):21037–48.
[6] Belleville P, Guillet F, Pons A, Deseure J, Merlin G, Druart F, Ramousse J, Grindler E. Low voltage water electrolysis:

decoupling hydrogen production using bioelectrochemical system. Int J Hydrogen Energy 2018;43(32):14867–75.
[7] Ismail MS, Ingham DB, Hughes KJ, Ma L, Pourkashanian M. Thermal modelling of the cathode in air-breathing PEM fuel cells. Appl Energy 2013;111:529–37.
[8] Baghalha M, Stumper J, Harvey D, Eikerling M. Modeling the effect of low carbon conductivity of the cathode catalyst layer on PEM fuel cell performance. ECS Trans 2010;28:113–23.
[9] Tamaki T, Wang H, Oka N, Honma I, Yoon SH, Yamaguchi T. Correlation between the carbon structures and their tolerance to carbon corrosion as catalyst supports for polymer electrolyte fuel cells. Int J Hydrogen Energy 2018;43(12):6406–12.
[10] Zhang X, Yang Y, Guo L, Liu H. Effects of carbon corrosion on mass transfer losses in proton exchange membrane fuel cells. Int J Hydrogen Energy 2017;42(7):4699–705.
[11] Jung J, Chung YH, Park HY, Han J, Kim HJ, Henkensmeier D, Yoo SJ, Kim JY, Lee SY, Song KH, Park HS, Jang JH. Electrochemical impedance analysis with transmission line model for accelerated carbon corrosion in polymer electrolyte membrane fuel cells. Int J Hydrogen Energy 2018;43(32):15457–65.
[12] Kusoglu A, Kwong A, Clark KT, Gunterman HP, Weber AZ. Water uptake of fuel-cell catalyst layers. J Electrochem Soc 2012;159:F530–5.
[13] Kundu S, Fowler M, Simon L, Grot S. Morphological features (defects) in fuel cell membrane electrode assemblies. J Power Sources 2006;157:650–6.
[14] Suzuki T, Murata H, Hatanaka T, Morimoto Y. Analysis of the catalyst layer of polymer electrolyte fuel cells. R&D Rev Toyota CRDL 2003;39:33–8.
[15] Gode P, Jaouen F, Lindbergh G, Lundblad A, Sundholm G. Influence of the composition on the structure and electrochemical characteristics of the PEFC cathode. Electrochim Acta 2003;48:4175–87.
[16] Morris DR, Liu SP, Gonzalez DV, Gostick JT. Effect of water sorption on the electronic conductivity of porous polymer electrolyte membrane fuel cell catalyst layers. ACS Appl Mater Interfaces 2014;6:18609–18.
[17] van der PAUW LJ. A method of measuring specific resistivity and Hall effect of discs of arbitrary shape. Philips Res Rep 1958;13:1–9.
[18] Koon DW, Knickerbocker CJ. What do you measure when you measure resistivity? Rev Sci Instrum 1992;63(1):207–10.
[19] Du C, Shi P, Cheng X, Yin G. Effective protonic and electronic conductivity of the catalyst layers in proton exchange membrane fuel cells. Electrochem Commun 2004;6:435–40.
[20] Ahadi M, Tam M, Saha MS, Stumper J, Bahrami M. Thermal conductivity of catalyst layer of polymer electrolyte membrane fuel cells: Part 1 – experimental study. J Power Sources 2017;354:207–14.
[21] Saha MS, Paul DK, Peppley BA, Karan K. Fabrication of catalyst-coated membrane by modified decal transfer technique. Electrochem Commun 2010;12:410–3.
[22] Jung CY, Kim WJ, Yi SC. Optimization of catalyst ink composition for the preparation of a membrane electrode assembly in a proton exchange membrane fuel cell using the decal transfer. Int J Hydrogen Energy 2012;37:18446–54.
[23] Cho HJ, Jang H, Lim S, Cho E, Lim TH, Oh IH, Kim HJ, Jang JH. Development of a novel decal transfer process for fabrication of high-performance and reliable membrane electrode assemblies for PEMFCs. Int J Hydrogen Energy 2011;36:12465–73.
[24] Suzuki T, Tsushima S, Hirai S. Effects of Nafion® ionomer and carbon particles on structure formation in a proton-exchange membrane fuel cell catalyst layer fabricated by the decal-transfer method. Int J Hydrogen Energy 2011;36:12361–9.
[25] Burheim OS, Su H, Hauge HH, Pasupathi S, Pollet BG. Study of thermal conductivity of PEM fuel cell catalyst layers. Int J Hydrogen Energy 2014;39(17):9397–408.
[26] Huang JY, Yasuda H, Mori H. Highly curved carbon nanostructures produced by ball-milling. Chem Phys Lett 1999;303:130–4.
[27] Chen Y, Gerald JF, Chadderton LT, Chaffron L. Nanoporous carbon produced by ball milling. Appl Phys Lett 1999;74:2782–4.
[28] Chen XH, Yang HS, Wu GT, Wang M, Deng FM, Zhang XB, Peng JC, Li WZ. Generation of curved or closed-shell carbon nanostructures by ball-milling of graphite. J Cryst Growth 2000;218(1):57–61.
[29] Li ZQ, Lu CJ, Xia ZP, Zhou Y, Luo Z. X-ray diffraction patterns of graphite and turbostratic carbon. Carbon 2007;45:1686–95.
[30] Yusof JM, Salleh MAM, Rashid SA, Ismail I, Adam SN. Characterisation of carbon particles (CPs) derived from dry milled kenaf biochar. JESTEC 2014:125–31.
[31] Zhang S, Cui Y, Wu B, Song R, Song H, Zhou J, Chen X, Liu J, Cao L. Control of graphitization degree and defects of carbon blacks through ball-milling. RSC Adv 2014;4:505–9.
[32] Li S, Liu S, Fu Z, Li Q, Wu C, Guo W. Surface modification and characterization of carbon black by sodium lignosulphonate. Surf Interface Anal 2017;49:197–204.
[33] Hamran N, Rashid AA. Effect of combination ultrasonic and ball milling techniques of commercial fillers dispersion on mechanical properties of natural rubber (NR) latex films. AIP Conf Proc 2017;1865, 040011.
[34] Leistenschneider D, Zürbes K, Schneidermann C, Grätz S, Oswald S, Wegner K, Klemmed B, Giebeler L, Eychmüller A, Borchardt L. Mechanochemical functionalization of carbon black at room temperature. Chimia 2018;4(1):14.
[35] Donnet JB, Bansal RC, Wang MJ. Carbon black: science and technology. 2nd ed. New York: CRC Press; 1993.
[36] Gray CA, Muranko H. Studies of robustness of industrial aciniform aggregates and agglomerates—carbon black and amorphous silicas: a review amplified by new data. J Occup Environ Med 2006;48:1279–90.
[37] Pollet BG, Goh JTE. The importance of ultrasonic parameters in the preparation of fuel cell catalyst inks. Electrochim Acta 2014;128:292–303.
[38] More K, Borup R, Reeves K. Identifying contributing degradation phenomena in PEM fuel cell membrane electrode assemblies via electron microscopy. ECS Trans 2006;3(1):717–33.
[39] Rashapov RR, Unno J, Gostick JT. Characterization of PEMFC gas diffusion layer porosity. J Electrochem Soc 2015;162(6):F603–12.
[40] Long CM, Nascarella MA, Valberg PA. Carbon black vs. black carbon and other airborne materials containing elemental carbon: physical and chemical distinctions. Environ Pollut 2013;181:271–86.
[41] Gray CA, Muranko H. Studies of robustness of industrial aciniform aggregates and agglomerates—carbon black and amorphous silicas: a review amplified by new data. J Occup Environ Med 2006;48:1279–90.
[42] Carbon black user's guide: safety, health, & environmental information. International Carbon Black Association (ICBA). 2006. www.carbon-black.org.
[43] Gostick JT, Fowler MW, Ioannidis MA, Pritzker MD, Volfkovich YM, Sakars A. Capillary pressure and hydrophilic porosity in gas diffusion layers for polymer electrolyte fuel cells. J Power Sources 2006;156:375–87.
[44] Bonifácio RN, Paschoal JOA, Linardi M, Cuenca R. Catalyst layer optimization by surface tension control during ink formulation of membrane electrode assemblies in proton

exchange membrane fuel cell. J Power Sources 2011;196(10):4680–5.
[45] Rubatat L, Diat O. Stretching effect on Nafion fibrillar nanostructure. Macromolecules 2007;40:9455–62.
[46] Van der Heijden PC, Rubatat L, Diat O. Orientation of drawn Nafion at molecular and mesoscopic scales. Macromolecules 2004;37:5327–36.
[47] Li J, Wilmsmeyer KG, Madsen LA. Hydrophilic channel alignment modes in perfluorosulfonate ionomers: implications for proton transport. Macromolecules 2008;41:4555–7.
[48] Metatla N, Palato S, Soldera A. Change in morphology of fuel cell membranes under shearing. Soft Matter 2013;9:11093–7.
[49] Jacobs CJ. Influence of catalyst ink mixing procedures on catalyst layer properties and in-situ PEMFC performance. Master's Thesis. Cape Town, South Africa: Department of Chemical Engineering, University of Cape Town; 2016.
[50] Rubatat L, Gebel G, Diat O. Fibrillar structure of Nafion: matching Fourier and real space studies of corresponding films and solutions. Macromolecules 2004;37:7772–83.
[51] Park MJ, Balsara NP. Anisotropic proton conduction in aligned block copolymer electrolyte membranes at equilibrium with humid air. Macromolecules 2010;43(1):292–8.
[52] Schmidt-Rohr K, Chen Q. Parallel cylindrical water nanochannels in Nafion fuel-cell membranes. Nat Mater 2008;7:75–83.
[53] Majewski PW, Gopinadhan M, Jang WS, Lutkenhaus JL, Osuji CO. Anisotropic ionic conductivity in block copolymer membranes by magnetic field alignment. J Am Chem Soc 2010;132(49):17516–22.
[54] Sobolyeva T. On the microstructure of PEM fuel cell catalyst layers. PhD Thesis, Science. Vancouver, Canada: Department of Chemistry, Simon Fraser University; 2010.
[55] Soboleva T, Zhao X, Malek K, Xie Z, Navessin T, Holdcroft S. On the micro-, meso-, and macroporous structures of polymer electrolyte membrane fuel cell catalyst layers. ACS Appl Mater Interfaces 2010;2(2):375–84.
[56] Holdcroft S. Fuel cell catalyst layers: a polymer science perspective. Chem Mater 2013;26(1):381–93.
[57] Li L. A characterization study on catalyst layers in proton exchange membrane fuel cells. PhD Thesis. Knoxville, United States: Chemical Engineering, The University of Tennessee; 2016.
[58] Cimenti M, Bessarabov D, Tam M, Stumper J. Investigation of proton transport in the catalyst layer of PEM fuel cells by electrochemical impedance spectroscopy. ECS Trans 2010;28(23):147–57.
[59] Lefebvre MC, Martin RB, Pickup PG. Characterization of ionic conductivity profiles within proton exchange membrane fuel cell gas diffusion electrodes by impedance spectroscopy. Electrochem Solid St 1999;2(6):259–61.
[60] Wu J, Melo LGA, Zhu X, West MM, Berejnov V, Susac D, Stumper J, Hitchcock AP. 4D imaging of polymer electrolyte membrane fuel cell catalyst layers by soft X-ray spectro-tomography. J Power Sources 2018;381:72–83.
[61] Bernardi DM, Verbrugge MW. A mathematical model of the solid-polymer-electrolyte fuel cell. J Electrochem Soc 1992;139(9):2477–91.
[62] Marr C, Li X. Composition and performance modelling of catalyst layer in a proton exchange membrane fuel cell. J Power Sources 1999;77(1):17–27.
[63] Um S, Wang CY, Chen KS. Computational fluid dynamics modeling of proton exchange membrane fuel cells. J Electrochem Soc 2000;147(12):4485–93.
[64] Mench MM. Fuel cell engines. Hoboken: John Wiley & Sons, Inc.; 2008.
[65] Avcioglu GS, Ficicilar B, Eroglu I. Improved PEM fuel cell performance with hydrophobic catalyst layers. Int J Hydrogen Energy 2018;43(40):18632–41.
[66] Cheng X, Yi B, Han M, Zhang J, Qiao Y, Yu J. Investigation of platinum utilization and morphology in catalyst layer of polymer electrolyte fuel cells. J Power Sources 1999;79(1):75–81.
[67] Boyer C, Gamburzev S, Velev O, Srinivasan S, Appleby AJ. Measurements of proton conductivity in the active layer of PEM fuel cell gas diffusion electrodes. Electrochim Acta 1998;43(24):3703–9.